

# 1 Anomalous Amide Proton Chemical Shifts as Signatures of Hydrogen 2 Bonding to Aromatic Sidechains

3 Kumaran Baskaran<sup>\*1</sup>, Colin W. Wilburn<sup>\*1</sup>, Jonathan R. Wedell<sup>1</sup>, Leonardus M. I. Koharudin<sup>2</sup>, Eldon L.  
4 Ulrich<sup>1</sup>, Adam D. Schuyler<sup>1</sup>, Hamid R. Eghbalnia<sup>1</sup>, Angela M. Gronenborn<sup>2</sup>, and Jeffrey C. Hoch<sup>1</sup>

5 <sup>1</sup>Department of Molecular Biology and Biophysics, UConn Health, 263 Farmington Ave., Farmington, CT 06030-3305 USA

6 <sup>2</sup>Department of Structural Biology University of Pittsburgh School of Medicine 3501 Fifth Ave., BST3/Rm. 1050 Pittsburgh, PA  
7 15260 USA

8 Correspondence to: Jeffrey C. Hoch ([hoch@uchc.edu](mailto:hoch@uchc.edu))

9 Dedicated to Professor Robert Kaptein on the occasion of his 80<sup>th</sup> birthday.

10 **Abstract.** Hydrogen bonding between an amide group and the p- $\pi$  cloud of an aromatic ring was first identified in a protein in the  
11 1980s. Subsequent surveys of high-resolution X-ray crystal structures found multiple instances, but their preponderance was  
12 determined to be infrequent. Hydrogen atoms participating in a hydrogen bond to the p- $\pi$  cloud of an aromatic ring are expected  
13 to experience an upfield chemical shift arising from a shielding ring current shift. We survey the Biological Magnetic Resonance  
14 Data Bank for amide hydrogens exhibiting unusual shifts as well as corroborating nuclear Overhauser effects between the amide  
15 protons and ring protons. We find evidence that Trp residues are more likely to be involved in p- $\pi$  hydrogen bonds than other  
16 aromatic amino acids, whereas His residues are more likely to be involved in in-plane hydrogen bonds with a ring nitrogen acting  
17 as the hydrogen acceptor. The p- $\pi$  hydrogen bonds may be more abundant than previously believed. The inclusion in NMR structure  
18 refinement protocols of shift effects in amide protons from aromatic side chains, or explicit hydrogen bond restraints between  
19 amides and aromatic rings, could improve the local accuracy of side-chain orientations in solution NMR protein structures, but  
20 their impact on global accuracy is likely to be limited.

## 21 1 Introduction

22 In 1986, Perutz et al. (Levitt and Perutz, 1988) identified a putative hydrogen bond between an amino group of Asparagine and an  
23 aromatic ring of a drug bound to hemoglobin. Similar observations of the  $\pi$  electrons of aromatic rings acting as acceptors for  
24 hydrogen bonding have been reported before and since. (Klemperer et al., 1954; Mcphail and Sim, 1965; Knee et al., 1987) Later  
25 in 1986, Burley and Petsko (Burley and Petsko, 1986) surveyed 33 high resolution protein structures and found further evidence  
26 of aromatic hydrogen bonds. Tüchsen and Woodward (Tüchsen and Woodward, 1987) subsequently observed an upfield shift in  
27 the Gly-37 NH and Asn-44 HN resonances due to a nearby Tyr-35 aromatic group. The measurements from this study allowed  
28 Levitt and Perutz (Perutz, 1993) to estimate that these interactions contribute around 3 kcal mol<sup>-1</sup> in stabilizing enthalpy, about  
29 half as strong as a conventional hydrogen bond. Further evidence of such H-bonding came from the 2001 study by Brinkley and  
30 Gupta (Brinkley and B., 2001) showing FTIR spectroscopic evidence for hydrogen bonding between alcohols and aromatic rings.  
31 The ability of aromatic rings to engage in weakly polar CH- $\pi$  interactions is well documented, with NMR data from Plevin et  
32 al. (Plevin et al., 2010) in the form of weak scalar (J) couplings between methyl groups and atoms in aromatic rings providing direct  
33 evidence of these interactions. The study also included a survey of 183 X-ray structures and found 183 putative Me/ $\pi$  interactions.  
34 Brandl et al. (Brandl et al., 2001) surveyed 1154 protein structures from the Protein Data Bank (PDB (Consortium, 2019) for C-H

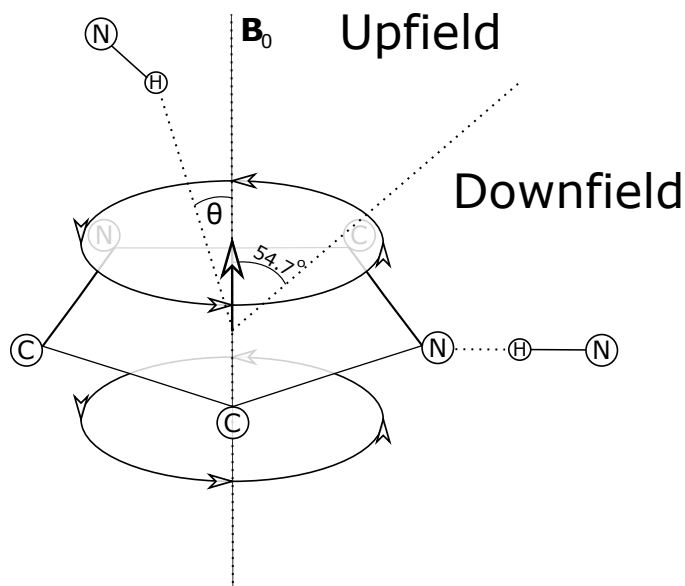
35  $\pi$  H bonds and found 14,087 involving aromatic rings and satisfying their geometric criteria. This is made all the more impressive  
36 when considering that Levitt and Perutz report the partial charges on the C–H group are one third those on the N–H group (the  
37 subject of this paper), suggesting that the interaction studied by Brandl et al. is correspondingly weaker. Another survey of note  
38 was performed by Weiss et al. in 2010.(Weiss et al., 2001) This complete hydrogen bond analysis of two high resolution protein  
39 structures from PDB found 50 C–H  $\pi$  and two (N,O)–H  $\pi$  bonds.

40 In addition to their ubiquity, there is some indication of the importance of these interactions. In a 1993 review, Perutz (Perutz,  
41 1993) indicated the potentially wide-ranging importance of these interactions, particularly Armstrong et al.'s demonstration of  
42 their role in stabilizing  $\alpha$ -helices(Armstrong et al., 1993). There is also evidence that similar interactions play an important role in  
43 protein-ligand complexes.(Panigrahi and Desiraju, 2007; Polverini et al., 2008)

44 Following the example of Tüchsen and Woodward (Tüchsen and Woodward, 1987) we seek to use NMR to provide corroborative  
45 evidence of aromatic hydrogen bonds. In this paper, we survey the Biological Magnetic Resonance Bank (BMRB) for unusual  
46 amide proton chemical shifts and amide-aromatic nuclear Overhauser effects.

47

48 Theoretical models for the geometrical dependence of the ring current shift include parameterization of quantum-mechanical(Haigh  
49 and Mallion, 1979; Memory, 1963) calculations, semi-classical approximation using the Biot-Savart Law(Jackson, 1999) for the  
50 field arising from current loops (Waugh and Fessenden, 1957; Jr. and Bovey, 1958), and a dipole approximation. For distances  
51 from the ring center that are greater than 3 Å above the plane of the ring, and 5 Å in the plane of the ring, the theories all agree  
52 well with a dipole approximation.(Hoch, 1983) The  $(1-3\cos^2(\theta))/r^3$  geometrical dependence of the field arising from a magnetic  
53 dipole (where  $\theta$  is the angle between the vector from a proton to the aromatic ring center and the vector normal to the plane of the  
54 ring) provides vivid explanation for cone separating upfield-shifted from down-field-shifted regions defined by  $\theta=54.7^\circ$  (Figure  
55 1).



56  
 57 **Figure 1.** Definition of the azimuthal angle ( $\theta$ ) and demarcation of regions of upfield and downfield ring current shifts.  
 58 For protons above the plane of a Tyr or Phe ring the upfield shift can reach 1.5 ppm for distances from the ring center around 3  
 59 Å; for protons in the plane of the ring the downfield shift approaches 2 ppm at 3 Å. For Trp the effects can be significantly larger.  
 60 Local mobility (e.g. fluctuations about the  $\chi_2$  side-chain dihedral angle of the aromatic residue) can substantially diminish ring  
 61 current shifts.<sup>21</sup>  
 62

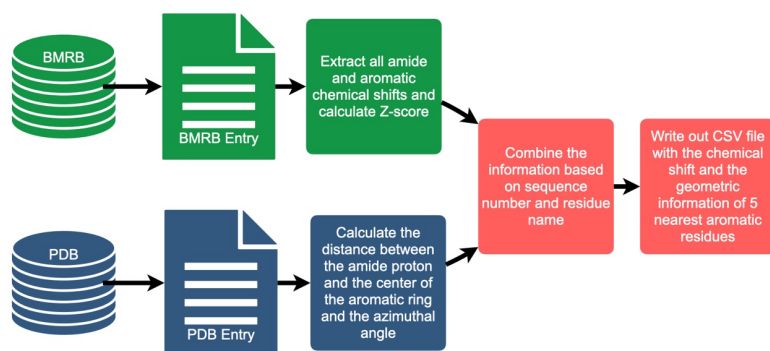
## 63 2 Approach

64 To investigate the connection between amide proton chemical shifts and the potential for hydrogen bonding to an aromatic ring,  
 65 we searched BMRB for assigned amide protons in proteins corresponding to structures deposited in the PDB. BMRB provides the  
 66 list of BMRB and PDB entry id pairs via BMRB API ([http://api.bmrbl.io/v2/mappings/bmrbl/pdb?match\\_type=exact](http://api.bmrbl.io/v2/mappings/bmrbl/pdb?match_type=exact)). As of Jan  
 67 2021 we found 7750 BMRB/PDB paired entries and retrieved the BMRB entries (in NMR-STAR format (Ulrich et al., 2019)) and  
 68 PDB entries (in mmCIF format (Bourne et al., 1997)) from their respective databases. We filtered out DNA/RNA entries, entries  
 69 with legends, oligomers and protein complexes. At the end we prepared a dataset consists of 363686 amide protons from 4670  
 70 entries. We combined the chemical shift information from BMRB and the geometric information from PDB for each amide proton  
 71 and its nearest aromatic ring using sequence number and residue name. For each assigned amide chemical shift, Z-score was  
 72 computed characterizing the deviation of the shift from its mean value from the BMRB database

$$73 \quad Z = \frac{\delta_{res} - \bar{\delta}_{res}}{\sigma_{res}} \quad (1)$$

74

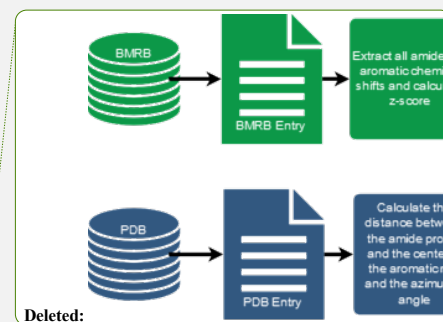
75 where  $\delta_{res}$  is the amide chemical shift of a given residue in ppm,  $\bar{\delta}_{res}$  and  $\sigma_{res}$  are the mean and the standard deviation of the amide  
76 proton of a given residue type, based on statistics maintained by BMRB ([https://bmrbl.io/ref\\_info/stats.php?restype=aa&set=fil](https://bmrbl.io/ref_info/stats.php?restype=aa&set=fil)).  
77 For each assigned amide, the distance from the amide position to the centre of the nearest aromatic ring is computed from the  
78 coordinates in the PDB mmCIF file. The distance is defined as the average of the distance from the amide proton to the centre of  
79 the aromatic ring, averaged over the members of the structural ensemble present in the PDB entry. For the nearest aromatic ring,  
80 we calculated an azimuth angle (Figure 1), defined as the angle between a vector normal to the aromatic ring plane and the vector  
81 between the amide proton and the centre of the ring. The ring normal vector is computed by calculating the cross product of two  
82 vectors on the plane of the ring (say the vector from the centre of the ring to CG and CD1). The table of assigned chemical shifts,  
83 Z-scores, distances to the nearest aromatic ring and azimuth angles is provided as a comma-separated text file (CSV file) in the  
84 supplementary information. The workflow used in the analysis is depicted in Figure 2.



85

86 **Figure 2:** Manual federation of BMRB and PDB via a customized workflow.

87 Corroboration of close proximity between an amide proton and an aromatic ring observed in PDB structures is found in assigned  
88 distance restraints based on nuclear Overhauser effects (NOEs) present in the BMRB entries. NMR restraint files from the PDB  
89 were parsed using PyNMRSTAR (Smelter et al., 2017) for NOE restraints between amide protons and aromatic ring protons of  
90 different residues. Because many files list NOEs under 'simple' distance restraints, these were included. Due to inconsistencies  
91 prevalent in the restraint data, several criteria were implemented to ensure some conformity in the restraints included in our  
92 analysis. This and other reasons for excluding entries from the restraints analysis are described in greater detail in Supplementary  
93 Table 1. Also discarded were individual distance restraints which reported only a lower distance bound or an upper distance bound  
94 greater than 6Å (as this is inconsistent with the nuclear Overhauser effect) and restraints that were ambiguously between more than  
95 two different residues (in order to simplify the analysis). Of the entries that remained, 2573 listed at least one restraint between an  
96 amide proton and an aromatic ring proton and 848 did not. For this section of the analysis, the June 2021 ReBoxitory data lake  
97 snapshots of BMRB and PDB available on NMRbox ([NMRbox.org./reboxitory/2021/06](https://nmrbox.org/reboxitory/2021/06)) were used.



Deleted: were downloaded

Deleted: and

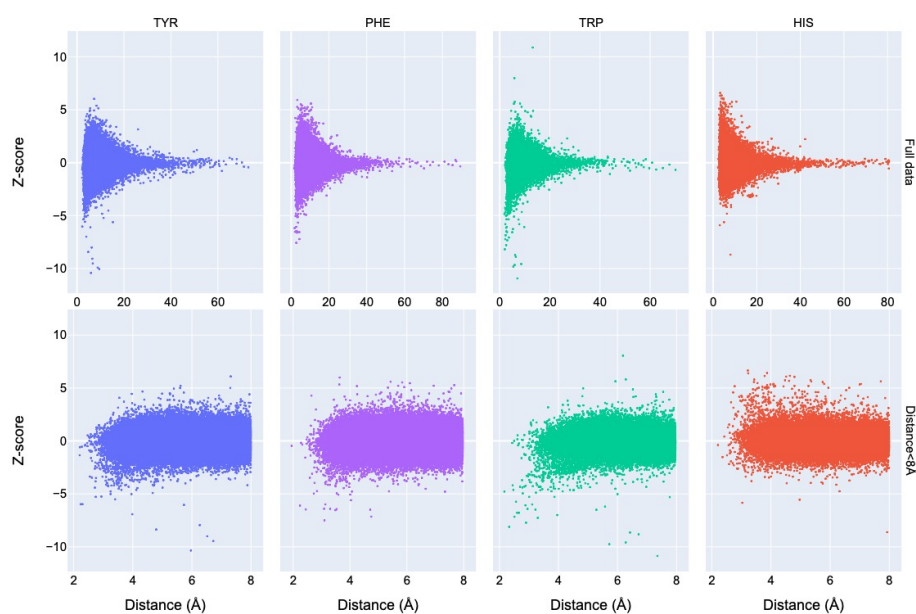
Deleted: 2564

Deleted: 863

103 **3 Results and Discussion**

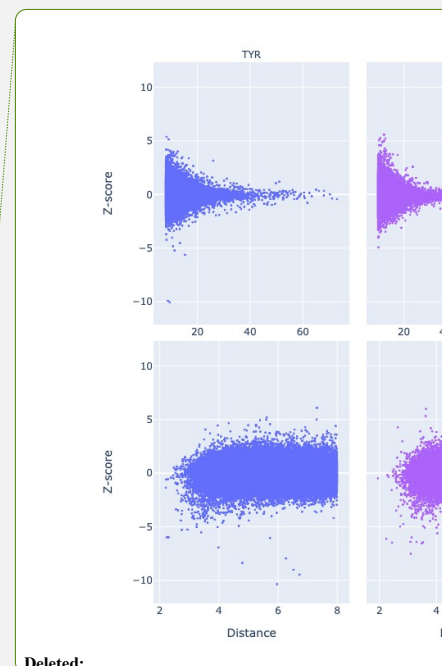
104 **3.1 Analysis of Chemical Shift Data**

105 Chemical shift Z-scores as a function of distance to the nearest aromatic ring are shown in Figure 3, separated by the type of  
106 aromatic sidechain. For all four aromatic residue types, there is a clear correlation between proximity to the aromatic ring and the  
107 amide chemical shift variance: significant deviations from the mean, corresponding to Z-scores greater than 2, are most likely  
108 when the proton is proximal to an aromatic ring, and the magnitude of the shift deviations are larger for closer proximity. The  
109 bottom row in Figure 3 examines the distribution of amide chemical shifts that are closer than 8 Å in greater detail.

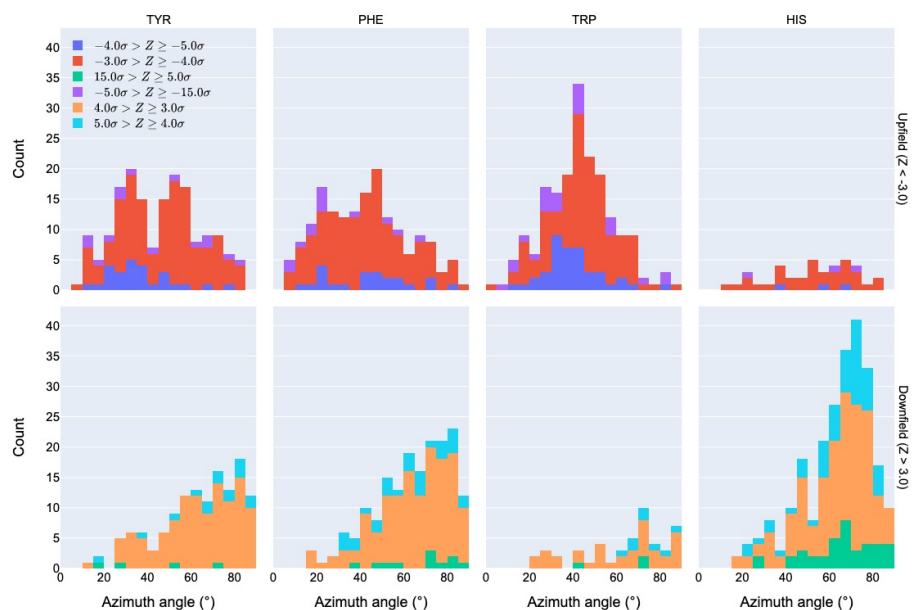


110 **Figure 3:** The distribution of amide chemical shifts as function of the distance of the amide proton from the center of the nearest  
111 aromatic ring.  
112  
113

114 The figure illustrates differences in the pattern of chemical shift deviation for the four different types of aromatic sidechains. For  
115 amide protons proximal to Phe, Tyr, or Trp sidechains, there is a noticeable preponderance of upfield shifts (negative Z-score). In  
116 contrast, His amide protons exhibiting large deviations from the mean tend to be shifted downfield (positive Z-scores). The  
117 difference in behavior of the outliers for the different aromatic residue types suggests the deviations are not simply the result of  
118 residues buried in the protein interior. The upfield-shifted resonances for amides proximal to Phe, Tyr, and Trp are consistent with  
119 hydrogen bonding between the amide and the p- $\pi$  electrons. The downfield-shifted resonances for amides proximal to His are  
120 consistent with hydrogen bonding to the electronegative nitrogen atoms of the His ring. In-plane downfield ring current shifts are  
121 the same sign as the expected downfield shifts arising from hydrogen bonding, with a predicted amide proton ring current shift of



123 0.5 ppm for an amide nitrogen distance of 3.4 Å. This is consistent with the observation of larger magnitude Z scores for downfield-  
 124 shifted amide protons proximal to His.

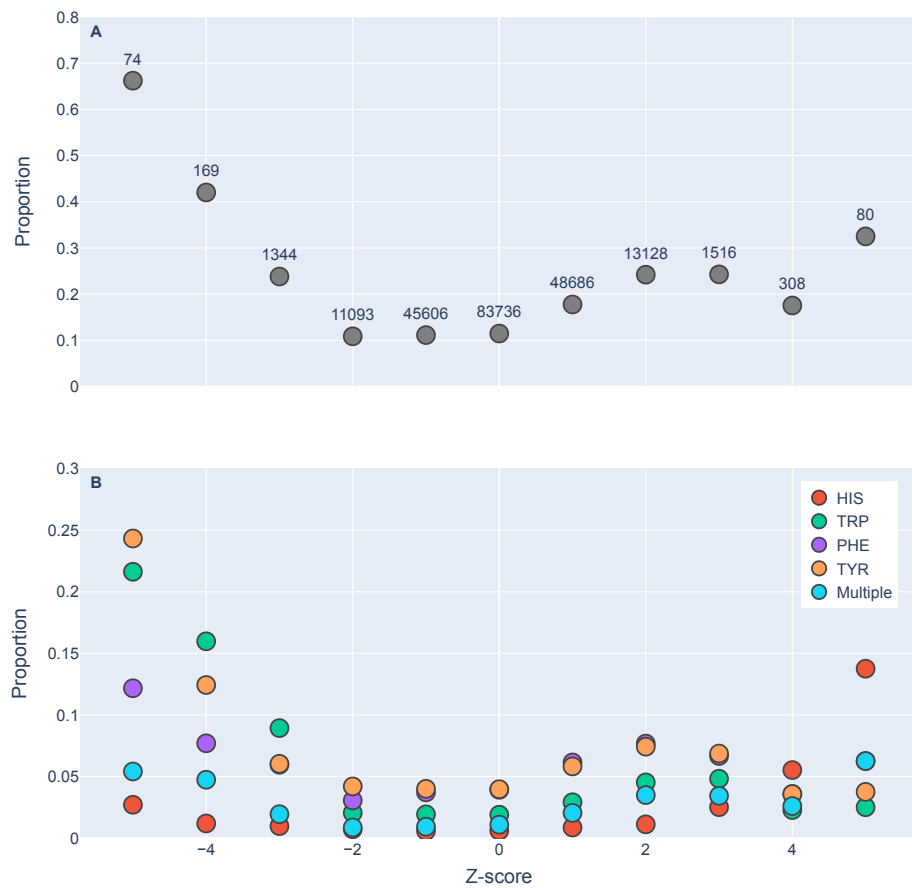


Deleted:

125  
 126 **Figure 4:** Distribution of azimuth angles for outlier ( $>3\sigma$ ) amide proton shifts. Upfield shifts are shown in the top row, downfield  
 127 shifts in the bottom row.

128  
 129 Further evidence of the unusual behavior of amide protons with unusual shifts proximal to His and Trp residues is found in their  
 130 spatial distribution. Figure 4 shows the distribution of azimuth angle for upfield and downfield outliers that are within 8 Å of an  
 131 aromatic ring. (Outliers are defined here as having absolute value of the Z-score greater than 3.) Shift outliers proximal to His tend  
 132 to reside near the ring plane, whereas shift outliers proximal to Trp tend to reside above the ring plane. Phe and Tyr don't exhibit  
 133 a pronounced preponderance of outliers above or near the ring plane. Interestingly, none of the maxima in the azimuth angle  
 134 distributions occur at 0°, expected for an amide proton directly above the ring centroid, nor 90°, expected for an amide proton lying  
 135 in the ring plane. The peaks near 25° observed for Tyr and Phe are close to the value expected for an amide proton 2.4 Å above  
 136 the ring plane and directly above one of the ring atoms, rather than above the ring centroid.

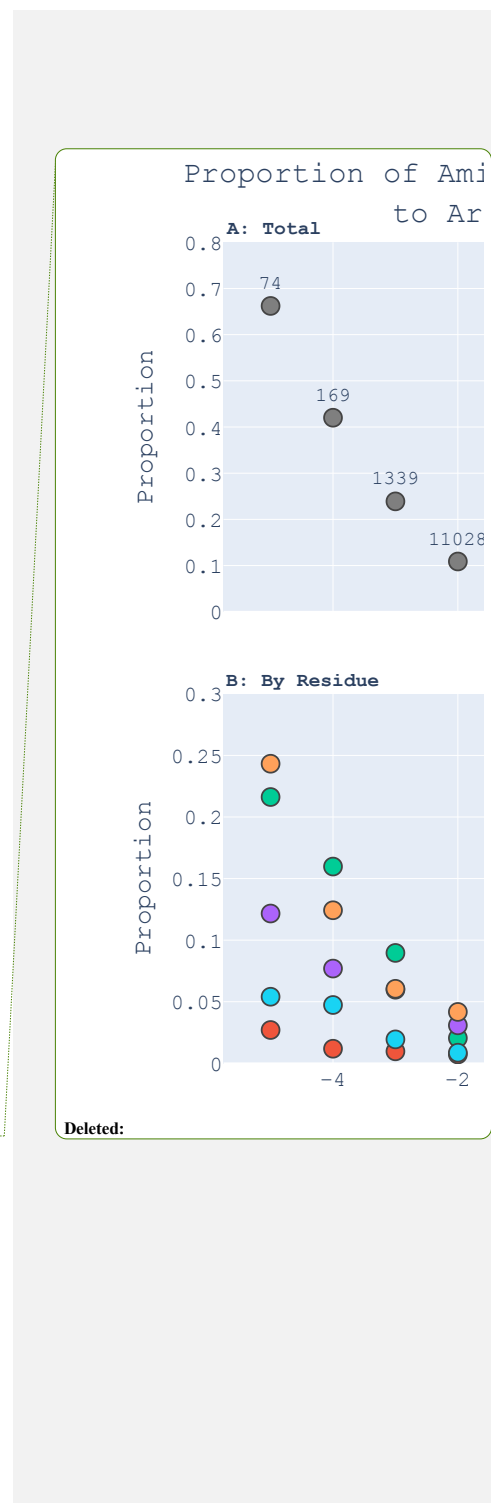
137



140

141 **Figure 5:** Proportions of amide protons with at least one NOE restraint to an aromatic ring proton (y-axis), as a function of the  
 142 Z-score of the amide proton (x-axis). Proportions are calculated with respect to the total number of amide hydrogens with chemical  
 143 shifts reported in entries with at least one amide-aromatic restraint. The numbers over each point in panel A are the total number  
 144 of such amides (including those lacking any NOE restraints to a nearby aromatic) with that Z-score. In panel B, the restrained  
 145 amide protons are further demarcated by the type of aromatic sidechain to which they are restrained.

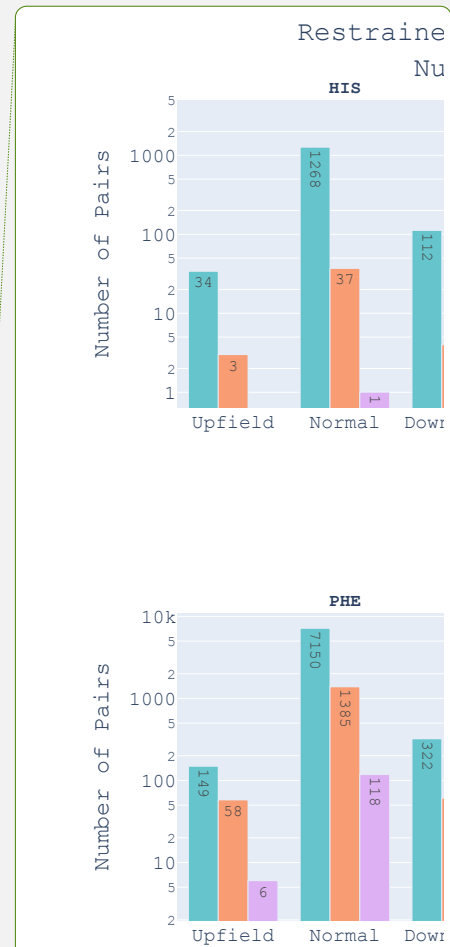
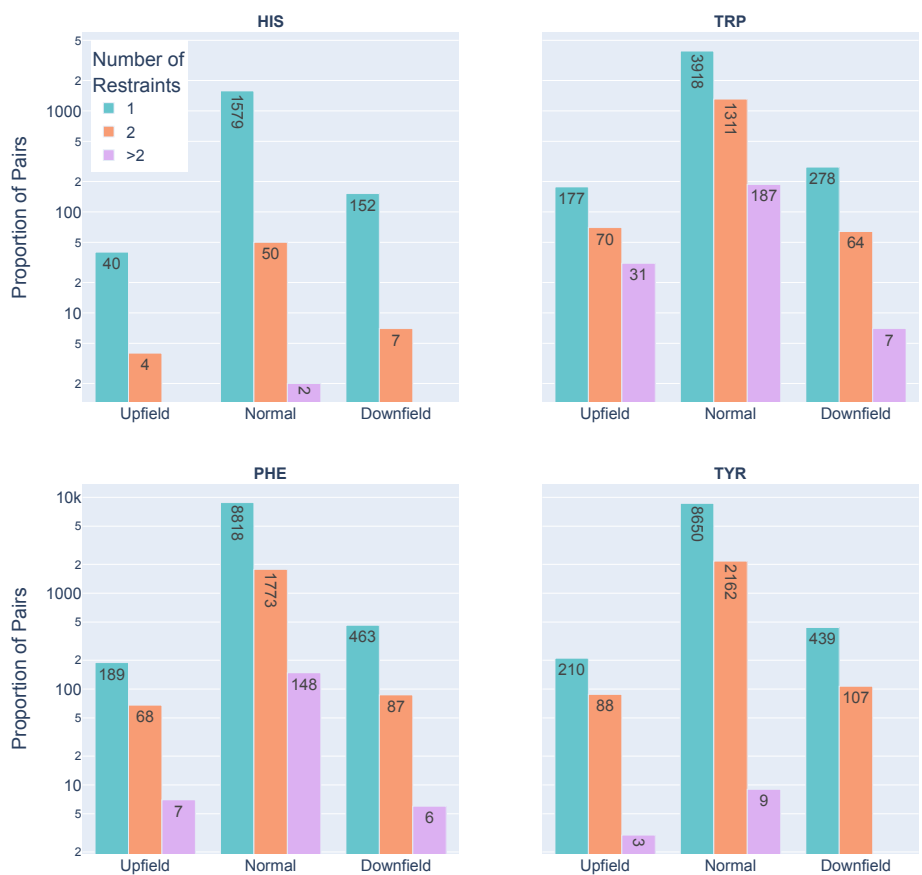
146



148 We found 31,859 amide protons with at least one NOE restraint to a nearby aromatic ring. Figure 5A shows the proportion of  
149 amide protons (from entries with usable restraint data and at least one amide-aromatic restraint) exhibiting these restraints. For  
150 both upfield- and downfield-shifted amide protons, the greater the deviation from the mean the greater the likelihood that  
151 corresponding NOE restraints are observed. The trend is noticeably more pronounced for the upfield-shifted amide protons, which  
152 is consistent with the formation of hydrogen bonds between the amide and the  $p-\pi$  electrons. The downfield-shifted amides exhibit  
153 a weaker correlation, which may be indicative of other dominating effects (not necessarily due to nearby aromatic rings). Figure  
154 5B further demarcates the data by the type of the nearby aromatic residue. We observe that the preponderance of amide-aromatic  
155 restraints in upfield-shifted amide protons for interactions with Trp and Tyr (and to a lesser extent Phe). In contrast, amide protons  
156 proximal to His residues predominate strong downfield shifts ( $Z \geq 4$ ). This stands as further evidence for hydrogen bonding from  
157 the amide to the  $p-\pi$  electrons in Trp, Tyr, and Phe, and to the nitrogen atoms in the His ring.

Deleted: 746





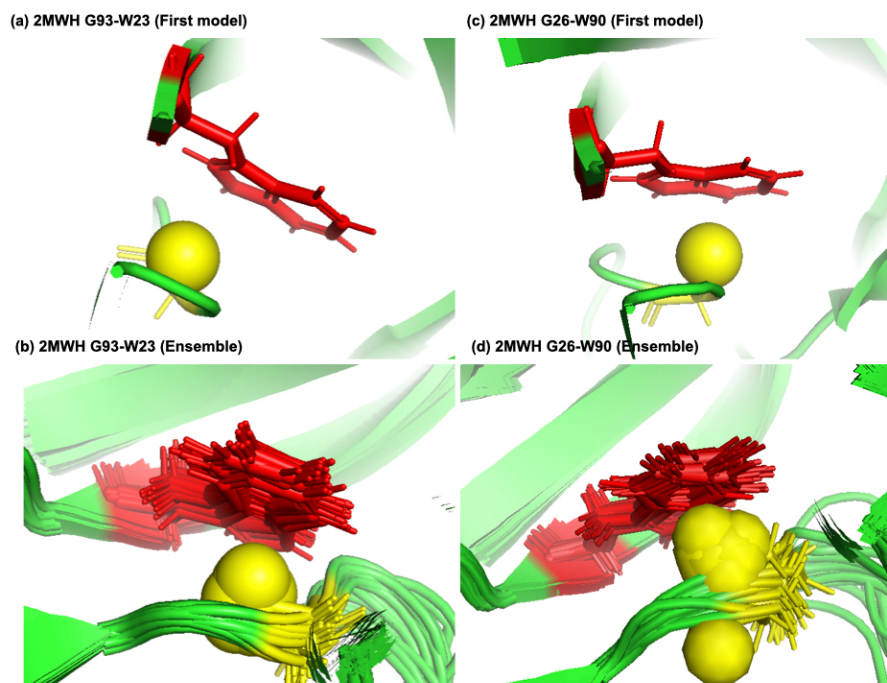
Deleted:

159  
 160 **Figure 6:** Shown are the number of restrained amide-aromatic pairs (that is amide protons and aromatic rings with at least one  
 161 defined restraint between them) for the four aromatic residue types and three Z-score classifications: upfield ( $Z \leq -2$ ), downfield  
 162 ( $Z \geq 2$ ), and normal ( $-2 \leq Z \leq 2$ ). The colors of the bars correspond to the number of restraints between the pairs; bar heights  
 163 are plotted using a logarithmic scale.

164  
 165 In Figure 6 the restrained amide-aromatic pairs are separated by the type of the aromatic residue and the number of restraints  
 166 between the amide proton and the aromatic ring protons. For every aromatic type, a greater proportion of the upfield-shifted pairs  
 167 have more than one restraint between them than the downfield-shifted pairs, which may indicate a hydrogen bond from the amide

to the p- $\pi$  electrons. his observation is consistent with the others. Finally, the prevalence of defined restrained pairs with an upfield outlier amide is quite high. From the 2529 entries considered, there were 887 such pairs, more than one in every three entries.

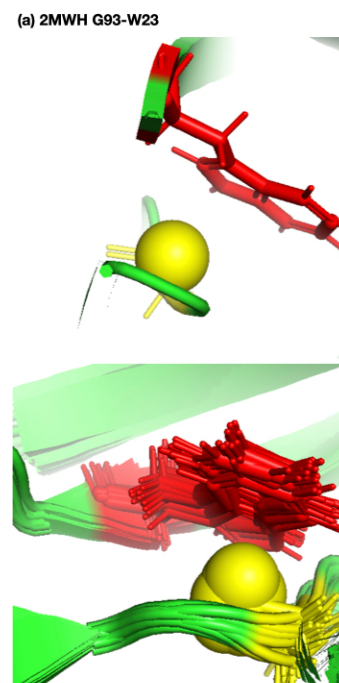
### 3.3 Examples



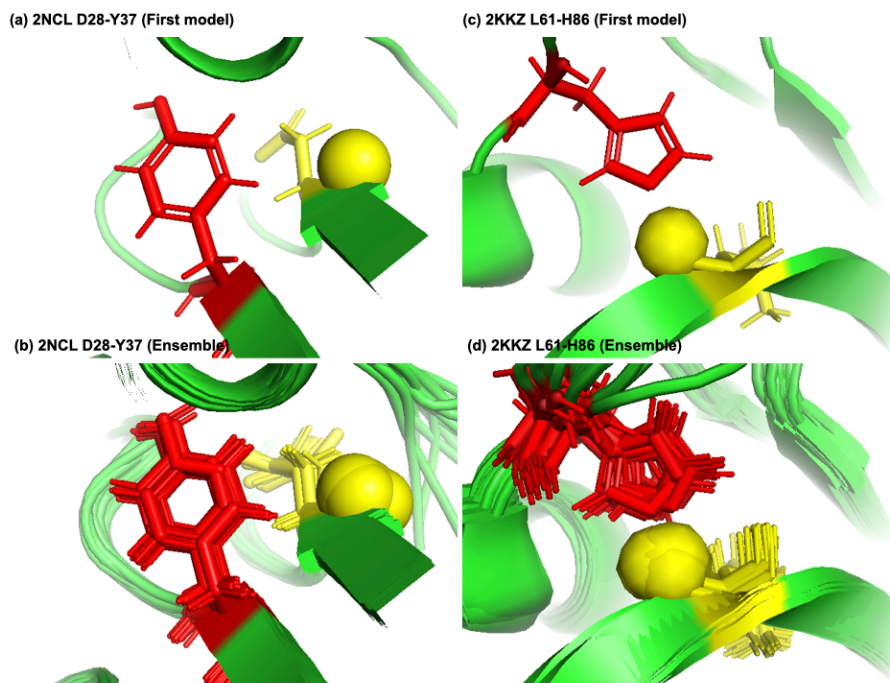
**Figure 7:** Examples of amide protons with extreme upfield shifts (a,b) PDB:2MWH The G93 amide proton is directly below the W23 aromatic ring ( $Z = -7$ ,  $\delta_{GLY} = 2.937$  ppm,  $d = 3.99 \text{ \AA}$ ,  $\theta = 43.9^\circ$ ,  $\delta_{GLY} = 8.237$  ppm,  $\sigma_{GLY} = 0.770$  ppm), (c,d) PDB:2MWH The G26 amide proton is directly below the W90 aromatic ring ( $Z = -6.43$ ,  $\delta_{GLY} = 3.38$  ppm,  $d = 2.98 \text{ \AA}$ ,  $\theta = 25.0^\circ$ ,  $\delta_{GLY} = 8.327$  ppm,  $\sigma_{GLY} = 0.770$  ppm). The amide proton is represented as a yellow sphere and the aromatic side chain is shown in red

Figure 7a & 7b shows the examples of p- $\pi$  hydrogen bond in the anti-HIV lectin *Oscillatoria agardhii* agglutinin (PDB ID:2MWH) in which the amide chemical shifts of G93 (z-score = -7,  $\delta_H = 2.937$  ppm) and G26 (z-score = -6.43,  $\delta_H = 3.38$  ppm) are upfield shifted due to the interaction of W23 and W90 respectively.

Deleted: 2523  
 Deleted: 1166  
 Deleted: were found, nearly  
 Deleted: such pair  
 Deleted: two  
 Deleted:



Deleted:  
 Deleted: ), (b  
 Deleted: ) . The top row shows only the first model and the bottom row shows the ensemble.  
 Deleted: **Figure 7:** Examples of amide protons with extreme upfield shifts (a,b) PDB:2MWH The G93 amide proton is directly below the W23 aromatic ring ( $Z = -7$ ,  $\delta_H = 2.937$  ppm), (b,  $d = 3.99 \text{ \AA}$ ,  $\theta = 43.9^\circ$ ,  $\delta_{GLY} = 8.237$  ppm,  $\sigma_{GLY} = 0.770$  ppm), (c,d) PDB:2MWH The G26 amide proton is directly below the W90 aromatic ring ( $Z = -6.43$ ,  $\delta_H = 3.38$  ppm) . The top row shows only the first model and the bottom row shows the ensemble.,  $d = 2.98 \text{ \AA}$ ,  $\theta = 25.0^\circ$ ,  $\delta_{GLY} = 8.327$  ppm,  $\sigma_{GLY} = 0.770$  ppm). The amide proton is represented as a yellow sphere and the aromatic side chain is shown in red

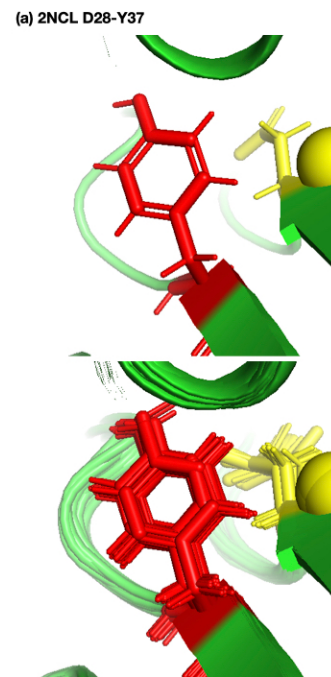


**Figure 8:** Examples of amide protons with extreme downfield shifts. (a,b) PDB:2NCL The D28 amide proton is near the plane of Y37 aromatic ring ( $Z=5.21$ ,  $\delta_{ASP} = 11.387$  ppm,  $d = 5.62 \text{ \AA}$ ,  $\theta = 72.0^\circ$ ,  $\delta_{LEU} = 8.299$  ppm,  $\sigma_{ASP} = 0.588$  ppm). (c,d) PDB:2KKZ The L61 amide proton forms a hydrogen bond with the side chain nitrogen of H86 ( $Z=6.66$ ,  $\delta_{LEU} = 12.56$  ppm,  $d = 3.22 \text{ \AA}$ ,  $\theta = 69.7^\circ$ ,  $\delta_{LEU} = 8.217$  ppm,  $\sigma_{LEU} = 0.735$  ppm). The amide proton is represented as a yellow sphere and the aromatic side chain is shown in red.

Figure 8a shows the amide proton of D28 is more or less on the plane of the Y37 aromatic ring in BOLA3 protein (PDB ID:2NCL) resulting the amide chemical shift of D28 ( $z\text{-score} = 5.21$ ,  $\delta_H = 11.387$  ppm) to shift downfield. Figure 8b shows an example of possible hydrogen bond between the NE2 of H86 and the amide proton of L61 in NS1 effector domain (PDB ID:2KKZ). As a result, L61 ( $z\text{-score} = 6.66$ ,  $\delta_H = 12.66$  ppm) amide chemical shift is strongly downfield shifted.

### 3.4 Bias, Structure, and Dynamics

Potential bias in the BMRB and PDB data likely undercounts the occurrence of aromatic hydrogen bonds. Absent assigned NOEs, the likelihood that an NMR structure will reflect a hydrogen bond to a  $\pi$  cloud of an aromatic ring is low, because the additive force fields used to refine most NMR structures, such as X-PLOR/CNS, do not capture the favorable interaction energy. To explore



Deleted:

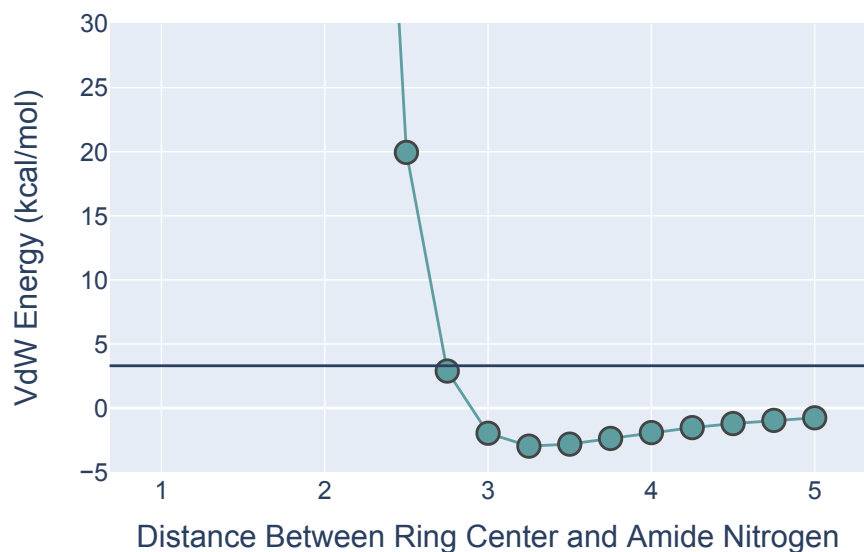
Deleted: ),(b)

Deleted: 66 ppm). The top row shows only the first model and the bottom row shows the ensemble.

Deleted: **Figure 8:** Examples of amide protons with extreme downfield shifts. (a,b) PDB:2NCL The D28 amide proton is near the plane of Y37 aromatic ring ( $Z=5.21$ ,  $\delta_H = 11.387$  ppm), ( $d = 5.62 \text{ \AA}$ ,  $\theta = 72.0^\circ$ ,  $\delta_{ASP} = 8.299$  ppm,  $\sigma_{ASP} = 0.588$  ppm). (c,d) PDB:2KKZ The L61 amide proton forms a hydrogen bond with the side chain nitrogen of H86 ( $Z=6.66$ ,  $\delta_H = 12.66$  ppm). The top row shows only the first model and the bottom row shows the ensemble. 56 ppm,  $d = 3.22 \text{ \AA}$ ,  $\theta = 69.7^\circ$ ,  $\delta_{LEU} = 8.217$  ppm,  $\sigma_{LEU} = 0.735$  ppm). The amide proton is represented as a yellow sphere and the aromatic side chain is shown in red.

Deleted: an pi

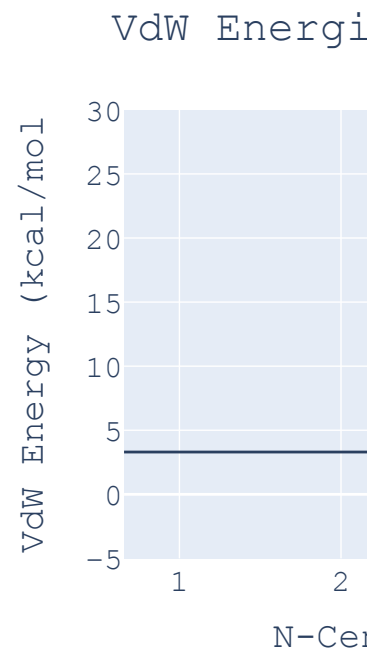
237 the Van der Waals interactions in an H-bonding geometry, we used MoSART(Hoch and Stern, 2003) to simulate ALA approaching  
238 PHE with the amide N-H of the former exactly aligned with the ring normal of the latter. The AMBER99 force field(Wang et al.,  
239 2000) was used to compute the energy.



240  
241 **Figure 9:** Van der Waals interaction energies for ALA approaching PHE with its amide N-H aligned with the ring normal. On the  
242 x-axis is the distance from the ALA nitrogen to the PHE ring center. VdW interaction energies for each distance were calculated  
243 by subtracting the VdW energies of ALA and PHE in isolation from the energies calculated at that distance from one another. All  
244 calculations were performed in MoSART using [the AMBER99 force field](#).

245  
246 The results, shown in Figure 9, agree with those presented by Levitt and Perutz(Levitt and Perutz, 1988): there is a local minimum  
247 in the van der Waals (VdW) energy with the amide nitrogen 3.3 Å from the ring center. The calculations also show that the non-  
248 bonded VdW interactions do not preclude adoption of a hydrogen-bonded aromatic ring, however the well depth is so small that  
249 the VdW attraction alone is likely insufficient to yield a favorable H-bond geometry without additional restraints.

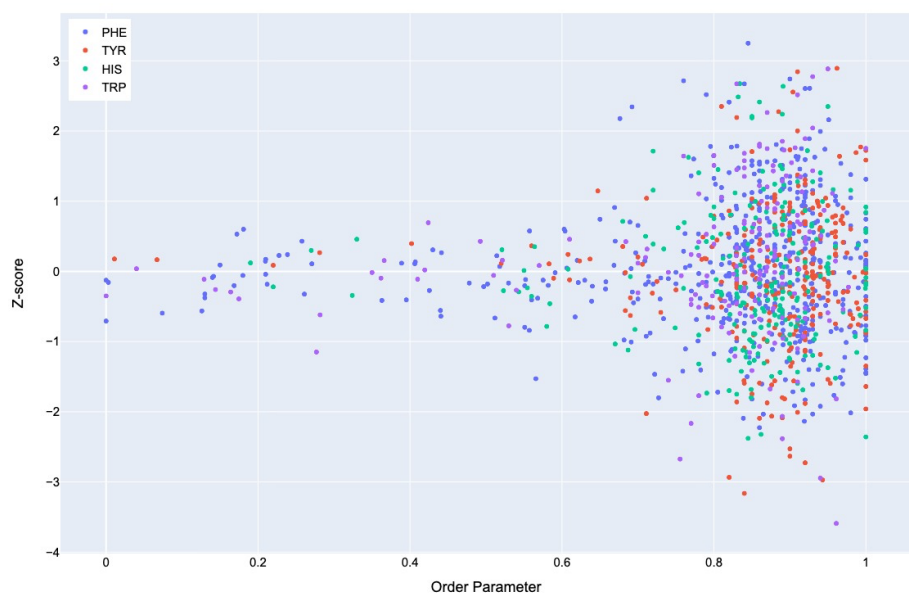
250 Lack of assignments are not evidence of the absence of an NOE. Missing assignments (for example, 6280 out of 8111 outlying  
251 amide proton shifts(|Z|>2) do not have assigned NOEs to an aromatic ring) also would lead to an undercount. Possible bias in  
252 BMRB notwithstanding, such as missing assignments not uniformly distributed, trends in shifts and NOE restraints for different



Deleted:

Deleted: fields

255 amino acid types that mirror one another provide a form of cross-validation and suggest that the shift outliers are not simply the  
256 result of being buried in the protein and thus easier to assign. Bias in PDB NMR structures could reflect current practice in structure  
257 refinement, which is dominated by restrained molecular mechanics simulations using empirical force fields augmented with  
258 experimental restraint potentials. The forms of these restraint potentials can introduce bias (Hoch and Stern, 2005), and the additive  
259 potentials that are used do not explicitly model p- $\pi$  hydrogen bonds. Absent NOE or ring current restraints, NMR structures are  
260 likely to under-represent aromatic hydrogen bonds.

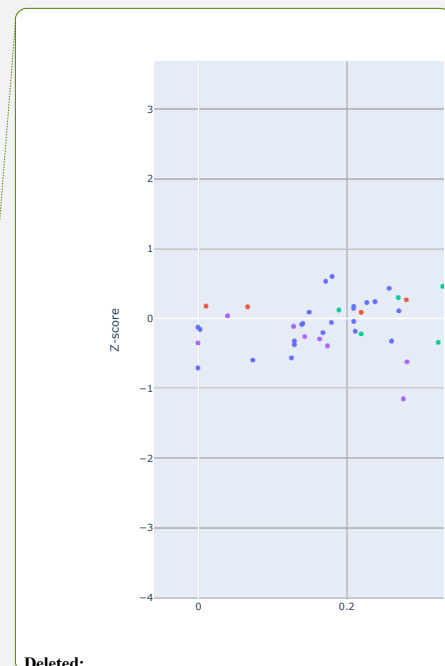


261

262 **Figure 10.** Correlation of Z-scores with order parameters.

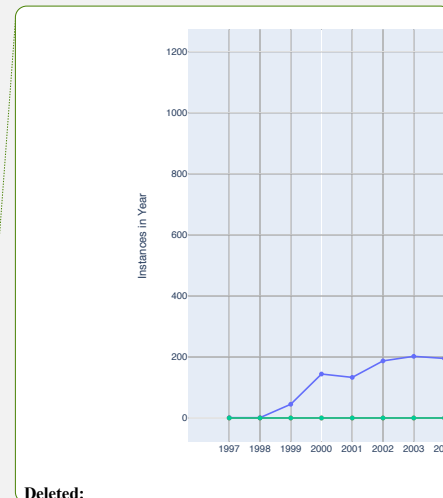
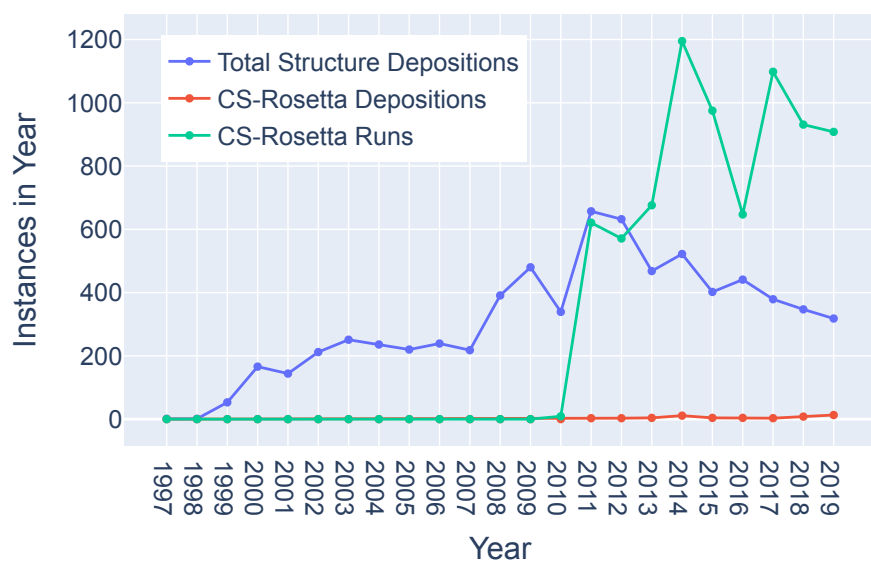
263

264 In general, dynamics and disorder render chemical shifts toward their random-coil or median values (Dass et al., 2020; Nielsen  
265 and Mulder, 2020). The correlation between secondary shift and order parameters is sufficiently strong that it has been used to  
266 predict order parameters from chemical shifts (Figure 10). (Berjanskii and Wishart, 2005) Ring current effects in particular are  
267 diminished by fluctuations about the  $\chi_2$  torsion angle. (Hoch et al., 1982) Hydrogen bonds involving aromatic rings should diminish  
268 these torsional fluctuations and should find correlates in side-chain relaxation properties for aromatic residues. Solution NMR  
269 structures in general tend to be more flexible than crystal structures (Fowler et al., 2020), and inclusion of hydrogen bonding  
270 interactions between amide groups and aromatic rings could reduce the flexibility and potentially improve the accuracy of NMR  
271 structures.



Deleted:

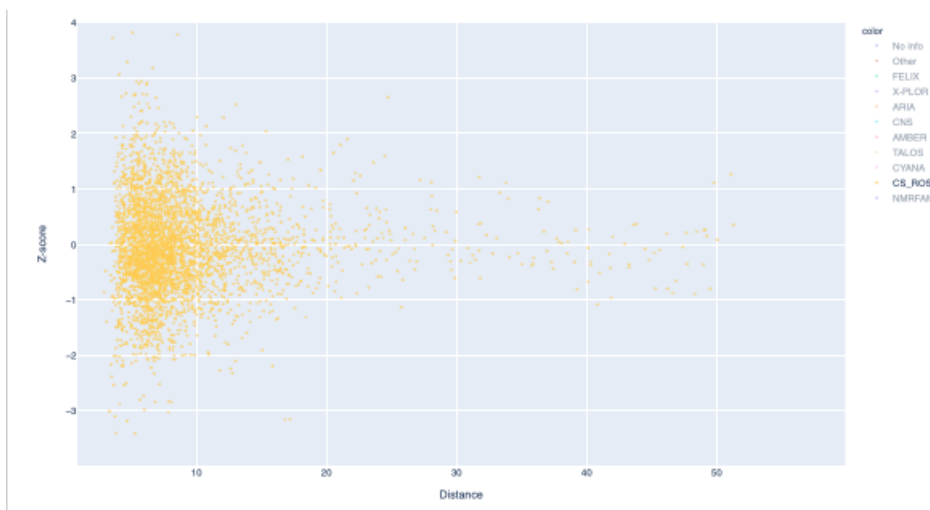
273 Although chemical shifts have been used to refine protein NMR structures (Shen et al., 2009; Berjanskii et al., 2015; Cavalli et al.,  
274 2007), for the most part these approaches leverage the influence of backbone torsion angles on chemical shifts, and do not consider  
275 the influence of nearby sidechains. Despite evidence that chemical shift refinement software is being used more frequently, the  
276 pace of chemical shift-refined structure depositions remains low (Figure 11).



Deleted:

277  
278 **Figure 11.** Trends in total BMRB structure depositions (blue), runs executed using the BMRB CS-Rosetta server (green), and  
279 depositions citing CS-Rosetta (red).

280  
281 Filtering the data plotted in Figure 3 to include only structures that reference CS-Rosetta (Figure 12) does not alter the overall  
282 distributions. A challenge confronting a deeper understanding of these effects is that the available metadata in BMRB does not  
283 articulate workflows, for example whether CS-Rosetta is used to generate initial trial structures or as a final refinement step), nor  
284 does it indicate when ring current shift restraints were utilized.



286

287 **Figure 12.** The distribution of amide chemical shifts for depositions citing C S-Rosetta as function of distance from the center of  
 288 the nearest ring (compare Figure 3).

#### 289 4 Concluding Remarks

290 Ring current shifts have a long history of providing structural insights from NMR studies of globular proteins (Perkins and Dwek,  
 291 1980), especially for methyl groups, whose secondary shifts tend to be dominated by ring current shifts. Early studies were largely  
 292 anecdotal, focusing on individual proteins or small surveys. While relatively dynamic aromatic rings (for example Tyr and Phe  
 293 rings that undergo ring flips on the fast exchange time scale) and disorder diminish the influence of ring current effects on secondary  
 294 shifts (Hoch et al., 1982), the accumulation of data in BMRB for folded proteins has provided a wealth of amide chemical shifts  
 295 exhibiting large secondary chemical shifts. Federation of BMRB chemical shift data with structural data from PDB confirms the  
 296 strong correlation between proximity to an aromatic ring and extreme secondary shifts. Markedly different secondary shift trends  
 297 for different aromatic residue types suggests promising avenues for improving [protein structure determination by NMR](#). Though  
 298 chemical shift refinement has been repeatedly demonstrated (Perilla et al., 2017), it has not yet been widely adopted.

299

300 The extreme outlier amide chemical shifts and corroborating NOE effects examined here provide strong evidence of the widespread  
 301 existence of amide-aromatic hydrogen bonds, but they are not fully conclusive. Nonetheless potential for under-representation in  
 302 the BMRB data exists because of incomplete assignments. Relaxation studies on ring dynamics, contrasting rings where evidence  
 303 suggests the presence of hydrogen bonding with rings lacking such evidence, could provide additional corroboration. Molecular  
 304 mechanics simulations and structure refinement using polarizable force fields could reveal additional aromatic hydrogen bonds  
 305 and restricted ring dynamics in folded proteins. We have initiated investigations along some of these lines.

306

307 More broadly, this preliminary investigation highlights the potential for unlocking latent knowledge hidden in BMRB, PDB, and  
 308 other biological databases. The challenges posed include curation and validation of the data repositories and federation of data

Deleted: proteins

310 between repositories. Robust and efficient solutions to these challenges are needed in order to realize the full promise of emerging  
311 methods in Machine Learning. (Hoch, 2019)

312

### 313 **5 Acknowledgements**

314 This work was supported by a grant from the Miriam and David Donoho Foundation, and by grants from the US National Institutes  
315 of Health (R01GM109046; P41GM111135) and from the University of Connecticut Office of the Vice President for Research  
316 (CARIC). We thank Milo Westler and Charles Schwieters for helpful discussions. We thank a reviewer for raising the question  
317 that led to understanding the significance of the peaks near 25° in the angular distributions.

318



319

320

321

322 **References**

323

- 324 Armstrong, K. M., Fairman, R., and Baldwin, R. L.: The (i, i + 4) Phe-His interaction studied in an alanine-based alpha-  
325 helix, *J Mol Biol*, 230, 284-291, 10.1006/jmbi.1993.1142, 1993.
- 326 Berjanskii, M., Arndt, D., Liang, Y., and Wishart, D. S.: A robust algorithm for optimizing protein structures with NMR  
327 chemical shifts, *J Biomol NMR*, 63, 255-264, 10.1007/s10858-015-9982-z, 2015.
- 328 Berjanskii, M. V. and Wishart, D. S.: A simple method to predict protein flexibility using secondary chemical shifts, *J*  
329 *Am Chem Soc*, 127, 14970-14971, 10.1021/ja054842f, 2005.
- 330 Bourne, P. E., Berman, H. M., McMahon, B., Watenpaugh, K. D., Westbrook, J. D., and Fitzgerald, P. M. D.: The  
331 Macromolecular Crystallographic Information File (mmCIF), *Methods in Enzymology*, 277, 571-590, 1997.
- 332 Brandl, M., Weiss, M. S., Jabs, A., Sühnel, J., and Hilgenfeld, R.: C-H...pi-interactions in proteins, *J Mol Biol*, 307, 357-  
333 377, 10.1006/jmbi.2000.4473, 2001.
- 334 Brinkley, R. L. and B., G. R.: Hydrogen bonding with aromatic rings., *AIChE Journal*, 47, 948-953, 2001.
- 335 Burley, S. K. and Petsko, G. A.: Amino-aromatic interactions in proteins, *FEBS Lett*, 203, 139-143, 10.1016/0014-  
336 5793(86)80730-x, 1986.
- 337 Cavalli, A., Salvatella, X., Dobson, C. M., and Vendruscolo, M.: Protein structure determination from NMR chemical  
338 shifts, *Proceedings of the National Academy of Sciences of the United States of America*, 104, 9615-9620,  
339 10.1073/pnas.0610313104, 2007.
- 340 consortium, w.: Protein Data Bank: the single global archive for 3D macromolecular structure data, *Nucleic Acids*  
341 *Res*, 47, D520-D528, 10.1093/nar/gky949, 2019.
- 342 Dass, R., Mulder, F. A. A., and Nielsen, J. T.: ODINPred: comprehensive prediction of protein order and disorder, *Sci*  
343 *Rep*, 10, 14780, 10.1038/s41598-020-71716-1, 2020.
- 344 Fowler, N. J., Sljoka, A., and Williamson, M. P.: A method for validating the accuracy of NMR protein structures, *Nat*  
345 *Commun*, 11, 6321, 10.1038/s41467-020-20177-1, 2020.
- 346 Haigh, C. W. and Mallion, R. B.: Ring current theories in nuclear magnetic resonance, *Progress in Nuclear Magnetic*  
347 *Resonance Spectroscopy*, 13, 303-344, [https://doi.org/10.1016/0079-6565\(79\)80010-2](https://doi.org/10.1016/0079-6565(79)80010-2), 1979.
- 348 Hoch, J. C.: The Influence of Protein Structure and Dynamics on NMR Parameters, *Chemistry*, Harvard University,  
349 1983.
- 350 Hoch, J. C.: If machines can learn, who needs scientists?, *J Magn Reson*, 306, 162-166, 10.1016/j.jmr.2019.07.044,  
351 2019.
- 352 Hoch, J. C. and Stern, A. S.: MoSART [code], 2003.
- 353 Hoch, J. C. and Stern, A. S.: Bayesian Restraint Potentials for Consistent Inference of Biomolecular Structure from  
354 NMR Data, 2005.
- 355 Hoch, J. C., Dobson, C. M., and Karplus, M.: Fluctuations and averaging of proton chemical shifts in the bovine  
356 pancreatic trypsin inhibitor, *Biochemistry*, 21, 1118-1125, 1982.
- 357 Jackson, J. D.: *Classical Electrodynamics*, 3rd, Wiley1999.
- 358 Jr., C. E. J. and Bovey, F. A.: Calculation of Nuclear Magnetic Resonance Spectra of Aromatic Hydrocarbons, *The*  
359 *Journal of Chemical Physics*, 29, 1012-1014, 10.1063/1.1744645, 1958.
- 360 Klemperer, W., Cronyn, M. W., Maki, A. H., and Pimentel, G. C.: Infrared studies of the association of secondary  
361 amides in various solvents., *J. Amer. Chem. Soc.*, 76, 5846-5848, 1954.
- 362 Knee, J. L., Khundkar, R. L., and Zewail, A. H.: Picosecond photofragment spectroscopy. iii. vibrational  
363 predissociation of van der waals' clusters., *J. Chem. Phys.*, 87, 115-127, 1987.
- 364 Levitt, M. and Perutz, M. F.: Aromatic rings act as hydrogen bond acceptors, *J Mol Biol*, 201, 751-754, 1988.

365 McPhail, A. T. and Sim, G. A.: Hydroxyl–benzene hydrogen bonding: an x-ray study., *Chem. Comm.*, 7, 124-126,  
366 1965.

367 Memory, J. D.: Ring Currents in Pentacyclic Hydrocarbons, *The Journal of Chemical Physics*, 38, 1341-1343,  
368 10.1063/1.1733855, 1963.

369 Nielsen, J. T. and Mulder, F. A. A.: Quantitative Protein Disorder Assessment Using NMR Chemical Shifts, *Methods*  
370 *Mol Biol*, 2141, 303-317, 10.1007/978-1-0716-0524-0\_15, 2020.

371 Panigrahi, S. K. and Desiraju, G. R.: Strong and weak hydrogen bonds in the protein-ligand interface, *Proteins*, 67,  
372 128-141, 10.1002/prot.21253, 2007.

373 Perilla, J. R., Zhao, G., Lu, M., Ning, J., Hou, G., Byeon, I. L., Gronenborn, A. M., Polenova, T., and Zhang, P.: CryoEM  
374 Structure Refinement by Integrating NMR Chemical Shifts with Molecular Dynamics Simulations, *J Phys Chem B*,  
375 121, 3853-3863, 10.1021/acs.jpcc.6b13105, 2017.

376 Perkins, S. J. and Dwek, R. A.: Comparisons of ring-current shifts calculated from the crystal structure of egg white  
377 lysozyme of hen with the proton nuclear magnetic resonance spectrum of lysozyme in solution, *Biochemistry*, 19,  
378 245-258, 1980.

379 Perutz, M. F.: The role of aromatic rings as hydrogen-bond acceptors in molecular recognition., *Phil. Trans. Royal*  
380 *Soc., Series A: Phys. and Eng. Sci.*, 345, 105-112, 1993.

381 Plevin, M. J., Bryce, D. L., and Boisbouvier, J.: Direct detection of CH/ $\pi$  interactions in proteins, *Nat Chem*, 2, 466-  
382 471, 10.1038/nchem.650, 2010.

383 Polverini, E., Rangaraj, G., Libich, D. S., Boggs, J. M., and Harauz, G.: Binding of the proline-rich segment of myelin  
384 basic protein to SH3 domains: spectroscopic, microarray, and modeling studies of ligand conformation and effects  
385 of posttranslational modifications, *Biochemistry*, 47, 267-282, 10.1021/bi701336n, 2008.

386 Shen, Y., Vernon, R., Baker, D., and Bax, A.: De novo protein structure generation from incomplete chemical shift  
387 assignments, *J Biomol NMR*, 43, 63-78, 10.1007/s10858-008-9288-5, 2009.

388 Smelter, A., Astra, M., and Moseley, H. N.: A fast and efficient python library for interfacing with the Biological  
389 Magnetic Resonance Data Bank, *BMC Bioinformatics*, 18, 175, 10.1186/s12859-017-1580-5, 2017.

390 Tüchsen, E. and Woodward, C.: Assignment of asparagine-44 side-chain primary amide  $^1\text{H}$  NMR resonances and the  
391 peptide amide N $^1\text{H}$  resonance of glycine-37 in basic pancreatic trypsin inhibitor, *Biochemistry*, 26, 1918-1925,  
392 10.1021/bi00381a020, 1987.

393 Ulrich, E. L., Baskaran, K., Dashti, H., Ioannidis, Y. E., Livny, M., Romero, P. R., Maziuk, D., Wedell, J. R., Yao, H.,  
394 Eghbalnia, H. R., Hoch, J. C., and Markley, J. L.: NMR-STAR: comprehensive ontology for representing, archiving and  
395 exchanging data from nuclear magnetic resonance spectroscopic experiments, *J Biomol NMR*, 73, 5-9,  
396 10.1007/s10858-018-0220-3, 2019.

397 Wang, Junmei, Ciepla, Piotr, Kollman, and A., P.: How well does a restrained electrostatic potential (RESP) model  
398 perform in calculating conformational energies of organic and biological molecules?, *J. Comp. Chem.*, 21, 1049-  
399 1074, 2000.

400 Waugh, J. S. and Fessenden, R. W.: Nuclear Resonance Spectra of Hydrocarbons: The Free Electron Model, *Journal*  
401 *of the American Chemical Society*, 79, 846-849, 10.1021/ja01561a017, 1957.

402 Weiss, M. S., Brandl, M., Sühnel, J., Pal, D., and Hilgenfeld, R.: More hydrogen bonds for the (structural) biologist,  
403 *Trends Biochem Sci*, 26, 521-523, 10.1016/s0968-0004(01)01935-1, 2001.

404